TEMPERATURE-BASED REACTIVE FLOW MODEL FOR ANFO

Roberta N. Mulford and Damian C. Swift
Los Alamos National Laboratory
Los Alamos, New Mexico 87545

Martin Braithwaite
Royal Military College of Science
Cranfield University
Shrivenham, Wiltshire, U.K.

Reaction rates depend on temperature as well as on the mechanical state. In shock wave initiation, experimental data almost always comprise mechanical measurements such as shock speed, material speed, compression, and pressure, and are accordingly modelled in terms of these parameters. Omission of temperature is one reason why mechanically based reaction rates do not extrapolate well outwith the range of states used to normalize them. The model presented addresses chemical processes directly, enabling chemical kinetic data reported in terms of temperature (and at STP, generally) to be used in shock reaction models. We have recently extended a temperature-based model for use with ANFO-type formulations. Reactive material is treated as a heterogeneous mixture of components, each of which has its own model for response to dynamic loading (equation of state, strength model, reactions.) A finite-rate equilibration model is used to determine the overall response of the mixture to dynamic loading. In this model of ANFO, the ammonium nitrate and the fuel oil are treated as separate components in the unreacted mixture.

INTRODUCTION

The detonation of ammonium nitrate / fuel oil (ANFO) explosive provides a demanding challenge to hydrocode modelling, as the multiple processes involved in the decomposition and reaction, coupled with the relatively long reaction zone compared to the charge size in many applications, make the performance of the explosive highly non-ideal [I]. Furthermore, ANFO-type explosives have a wide variations in composition, particle size and porosity, making it desirable to be able to predict the initiation and performance properties without having to re-calibrate the reactive flow model for each variant.

The objective of this work was to develop models to predict the initiation and blast behaviour, and capable of treating variations in composition and morphology, and different loading conditions. We found previously [2, 3] that it was important to use a reactive flow model based on sound physical processes in order to achieve a reasonable predictive capability. We describe here the structure and calibration of a model which represents the actual physical structure of ANFO explosive in simplified form, and which uses temperature-dependent reaction rates.

Because chemical kinetics is governed primarily by temperature, we have attempted to model reaction as a function of temperature, rather than just pressure. Previous investigation of military explosives [2, 3] indicated that this type of reaction model can adequately describe initiation of these explosives, accurately modelling both chemical reactions and heating from pore collapse ("hotspot" terms.) These models reproduced multiple-shock initiation behavior much more

accurately than did reactive flow models with a purely mechanical reaction rate, and they were also capable of being used to simulate cook-off problems. This type of model should be particularly valuable in simulating the behavior of non-ideal explosives such as ammonium nitrate(AN,) where some or all of the chemical reactions are not prompt at the pressures studied.

Fundamental data and physically-based models are of particular value in evaluating candidate methods for desensitising a mixture by altering its composition, as these may typically involve a wide range of materials and states. Physical and performance data may be scarce for some of these systems. However, chemical reactivity data such as rates, activation energies, and heats of reaction may be readily available or easily estimated.

There is a relative paucity of data on initiation in ANFO formulations, so our calibrations and simulations to date are to an extent sensitivity studies of a set of equations. More experiments are needed before the model can be regarded as accurate for predictive work.

PHYSICAL PROCESSES AND CHEMICAL REACTIONS

Thermal terms govern the chemical kinetics in any explosive, at the molecular level. Our previous studies have shown that temperature-based reaction rates can be used reliably, if heterogeneities are taken into account in an adequate way. [2, 3] The resulting reactive flow models have a better predictive capability than simpler empirical models. This makes them valuable for formulations such as AN, and oxidizer-fuel mixtures where the composition, morphology, and porosity can vary widely.

In non-ideal explosives such as AN, the chemical reactions may not be prompt or simple, and consequently the observed behavior of the system may be governed not by reaction which correlates simply with pressure at the wave front, but by a reaction of chemical components which is slow relative to shock processes. The dominant effects may be the slow mixture or reaction of products from two or more components, or by delayed reactions; multi-step reactions in which energy is evolved in late steps.

The mechanism that we propose for AN proceeds roughly by the following steps. Upon shocking the AN is heated by the passage of the shock, and may melt. This heating arises from deformation of the bulk solid, from compression of gas in the pores in the material, and from plastic flow or brittle fracture in the solid. Once sufficiently heated, the AN reacts with a temperature-dependent rate, heating itself, the fuel oil and the products. The hot fuel oil reacts with the oxygen-rich products of the AN decomposition. The fuel oil reaction may be considered in a number of ways. The AN may be intimately mixed with the fuel oil during passage of the shock. The fuel oil may evaporate, and the vapor react in the gas phase with the product gases from AN. The fuel oil may undergo thermal decomposition to products, which react in the gas phase with the product gases from the AN. We chose this pathway, assigning an Arrhenius rate to fuel oil decomposition, but assuming instantaneous reaction of the fuel oil products with the products of AN. The fuel oil may also react with the product gases by surface-burning, a mechanism differing from the first mechanism in its rate, which is described by a flame front rather than an Arrhenius form.. Finally, oxygen-rich species could diffuse into the fuel oil and react *in situ.* We neglect this pathway as condensed fuel oil is less likely to react than is the vapour, and the diffusion rate for molecules of fuel oil or its decomposition products is likely to be higher in the hot products than *vice versa*

Porosity and pore-size are related to the grain size of solid components, and consequently the grain size affects reaction, by altering the density of potential hotspots, while reducing their size. Smaller voids are known to be ineffective in producing reaction because rate-dependent strength makes smaller voids more difficult to compress, and because the greater surface area to volume ratio of small hotspots permits them to cool faster. We use thermal diffusion as a measure of grain size within the model.

As with other explosives, the porosity of the AN has been observed experimentally to make a difference in its reactive behavior. Several mechanisms may contribute to enhanced reaction of the AN at pores. P-V heating is the most obvious term, but our previous work indicates [3] that neither bulk heating alone, nor a model with enhanced reaction in the heated zone around a collapsed pore is sufficient to mimic observed reaction rates in HMX-based explosives. Other mechanisms that may be active are plastic work or else brittle fracture in the material around the pore. Plastic work appears to be an important heating mechanism in military explosives. [2, 4] A model based on plastic work has been developed for AN. [5] Brittle fracture is possible given the ceramic nature of AN, and might contribute to the heating. [6] The importance of viscosity and resulting energy delocalization in hotspot behavior has been

discussed. [2]

A term for plastic work should ideally be included in a model of this type. While some effort has gone into treating this term, plastic work at pores is not currently included in this model. [7]

Shear bands that form in response to the shock are a mechanism for localization of the mechanical energy of the shock. Lattice defects may cause delocalization of energy at a smaller scale. Formation of shear bands is greatest when the material, or a component, such as AN, is brittle.

REACTIVE FLOW MODEL

Ideally a reactive flow model should treat chemical processes with fidelity to the rates and energy releases expected for the system, sufficient to determine the rate-governing step under different stimuli, by describing the mechanical properties, and the distribution of the thermo-mechanical state for each spatially distinct phase in the composition.

The model used here attempts to provide enough freedom to model the initiation and reactive behavior of many explosives, while maintaining computational efficiency. The model approximates some relevant microstructural processes, without treating them fully. Initial values for most parameters were obtained from the composition, heats of formation, and other measured properties of the unreacted explosive, rather than by calibration against dynamic experiments.

Since the model was designed for use in continuum mechanics, it consists of a local state (varying with location and time inside a material subjected to dynamic loading) and a description of the material response (the same throughout a particular material). The material response model uses the local state to calculate 'external' properties such as mass density, stress and temperature, and to calculate the evolution of the state given applied loading and heating conditions. For an unreactive material, the simplest such model uses the density and energy to define the local state, and the eqation of state (EOS) as the response model. For reactive materials, our local state comprises the internal state and volume fraction for each spatially distinct region in the microstructure. This is therefore a heterogeneous mixture model. The material response includes the model for each component of the heterogeneous mixture, and a set of reaction rates. The reaction rates are used to transfer material between components, and also to describe reaction within a component if appropriate. The state and material response in each component depend on the material type used: it may be a traditional EOS, a thermodynamically complete EOS taking density and temperature as its local state, a constitutive model including strength or viscosity, or a homogeneous mixture of chemical components.

Since each component has its own state, the pressure and temperature can be calculated for each component. Pressure and temperature are equilibrated explicitly according to a separate time constant for each. This produces separate exponential approaches to mechanical and thermal equilibrium. Ideal equilibration can be enforced by setting the time constants to a small value. Pressure equilibration was performed by adjusting the volume fraction of each component towards equilibrium, and expanding or compressing along an isentrope. Temperature equilibration was performed by transferring heat energy at constant volume. The timescales were estimated from the grain size and properties of each component. In principle, they could be considered as additional continuum variables and evolved according to other microstructural processes.

Porous materials were represented by starting with a non-zero volume fraction of products. This model is not appropriate for all circumstances, but it was found to be reasonable for pores containing low density gas such as air.

An Arrhenius rate law was used, as probably the most physical representation of the chemical reaction process at the molecular level. 'Bulk' and 'surface' reactions were included, using the same reaction rate, but with the temperature of the adjacent component in the surface reaction. Whenever the surface reaction rate was predicted to be significant, material was burnt using a flame propagation model. The surface term included a description of the contact area between pairs of components in the heterogeneous mixture, estimated from the initial grain sizes and the volume fractions present at any stage in the reaction.

For ANFO itself, the heterogeneous components considered were AN, fuel oil, and gaseous products. AN and fuel oil were described by thermodynamically complete EOS, discussed later. The products were represented by a thermodynamically complete EOS for ANFO of various compositions, calculated using the CHEETAH chemical equilibrium program. [26]

The decomposition of AN was modelled by an Arrhenius rate law, transferring material to the products region. Decomposition of the fuel oil was represented by an additional Arrhenius rate, again with surface reactions. The composition of the products was altered as fuel oil was added. Reaction between AN products and decomposed

fuel oil was assumed to be instantaneous.

The initial porosity was treated explicitly using the mixture model, by including a heterogeneous component comprising pore gas. The pore gas was modelled an initial fraction of reaction products, which we found previously [3] to represent air with adequate accuracy. Pore collapse gave increased heating and thus increased the reaction rate principally through the surface terms.

A Lagrangian hydrocode was used to simulate dynamic experiments and hence allow the models to be evaluated against experimental data. The hydrocode used a finite difference representation of the continuum equations, integrating the hydrodynamics with a predictor-corrector scheme. Shock waves were stabilised with Wilkins' bulk artificial viscosity. Reaction was operator-split from the hydrodynamics and sub-cycled, using a forward-time integration scheme. Equilibration of pressure, temperature equilibration and chemical reactions were operator-split from each other and sub cycled.

EQUATION OF STATE FOR CONDENSED PHASES

Temperatures should be reasonably accurate in order to use a temperature-dependent reaction rate. A reliable value of heat capacity at STP varies with estimate to be made, but heat capacity depends on temperature and density. The temperature dependence arises from the population of modes available for absorbing thermal energy: phonons in solids and vibrations in molecules. A careful treatment of the population of these modes as a function of the energy of the mode was made, in order to provide an EOS which included a reasonably justifiable temperature.

The equation of state for condensed phases was quasiharmonic, consisting of a cold curve (or T = 0 isotherm) and a set of non-interacting modes corresponding to vibrational, rotational, and translational degrees of freedom. The cold curve was defined in terms of the variation of specific internal energy e_c with mass density ρ. Given $e_c(\rho)$, the cold curve pressure p_c can be found readily from

$$p_c(\rho) = - de_c/dv \qquad (1)$$

where v is the specific volume, 1/ρ. A set of vibrational modes $\{\omega_i(\rho)\}$ was considered. Given the cold curve and the $\{\omega_i\}$, the specific internal energy can be found for all states from

$$e(\rho, T) = e_c(\rho) + \frac{1}{m}\sum_i \hbar\omega_i(\rho)\{\exp(-\hbar\omega_i(\rho)/k_BT)-1\}^{-1} + \frac{1}{2} \qquad (2)$$

which is the energy of a set of oscillators with Bose-Einstein statistics. Similarly, the pressure can be found from

$$p(\rho, T) = p_c(\rho) + \frac{1}{m}\sum_i \hbar\frac{d\omega_i}{dv}\{\exp(-\hbar\omega_i(\rho)/k_BT)-1\}^{-1} + \frac{1}{2} \qquad (3)$$

These functions were used to generate SESAME-style tables [8] for more efficient computation. Previously, [27] when computed in-line, the equations of state were used in an explicit *(p, T)* form in the reactive flow program: the state in these materials was represented by its density and temperature rather than density and internal energy. As mechanical work or heat was applied to an element of material, the temperature was allowed to evolve according to the appropriate value of its specific heat capacity, $c_v = de/dT|_v$ calculated from the expression for *e(p, T)* above. A predictor-corrector scheme was used for second-order accuracy, and the scheme was sub cycled with a specified limit on temperature change in each cycle.

Ideally, the quasiharmonic equation of state would be calibrated using a cold curve and a set of frequencies (including their individual variation with compression), obtained from a rigorous theoretical model or direct experimental measurements. Unfortunately, neither source of data was available for the condensed components of ANFO. Instead, the cold curve was estimated from the shock Hugoniot, and the vibrational modes were obtained from the literature [9, 10] or estimated from the structure of each molecule. [10]

The cold curve was inferred by using a mechanical equation of state fitted to measured states on the shock Hugoniot, and assuming a simple model for off-Hugoniot states. A value was assumed for the density at $T = 0$, the specific internal energy necessary to give $p = 0$ was found from the mechanical equation of state, and the equation of state was integrated at constant entropy to estimate $e_c(\rho)$. This method has been applied previously to nitromethane, and performed well. [11] The Steinberg form [12] of Grüneisen equation of state was chosen for its computational convenience, taking $\Gamma = 2 s_i - 1$ [13].

For the molecules of interest, values of $\{\omega_i\}$ were estimated at STP from the structure of each

molecule. The accuracy of the modes was evaluated by comparing with the measured heat capacity at STP, or its variation with temperature. The variation with compression was estimated by assuming that $\gamma_i = (v/\omega_i)\, d\omega_i /dv$ constant for each mode, and equal for all modes. The value of this logarithmic derivative was calculated by finding the value which, when the corresponding quasiharmonic modes were added to the cold curve, reproduced the original STP state. The form assumed for the γ_i implies that the frequencies vary as

$$\omega_i(v) = \alpha exp(-\Gamma_i\, v/v_0). \qquad (4)$$

This is arguably a better-justified form than the linear variation with density which has been used for nitromethane [16] and is presumably valid over a smaller range of compressions.

The change in frequency as a function of pressure is in general slightly different for each vibrational mode [19], but none of these sensitivities could be determined explicitly in the absence of high pressure spectra. Instead, we assumed a single constant value for the logarithmic derivative of all the frequencies and determined it by iteration to reproduce the STP state.

EQUATIONS OF STATE FOR AMMONIUM NITRATE

Hugoniot data for AN have been reported previously. [17,18] The data of Courchinoux and Lalle were selected and used to calibrate a Steinberg-style Grüneisen EOS. The EOS parameters from a linear $u_s - u_p$ fit were c_0=1.8 km/s, s_1 =1.8, and Grüneisen's Γ = 2.6. The cold curve was obtained from this EOS.

The STP density for solid AN was taken to be 1.728 g/cm^3 —a median value from the data. A compression of 2.5% was assumed between STP and 0 K, giving a density of 1.7712 g/cm^3. Compared with the Hugoniot, the cold curve was not very sensitive to the density assumed at 0 K.

The 21 vibrational frequencies of ammonium nitrate were estimated from the frequencies of ammonium ion [9], the frequencies of nitrate ion, [9] nitric acid $HONO_2$, and salts $FONO_2$ and $ClONO_2$. [10] The only mode diverging appreciably from the template spectra is that of the N-O stretch,. This was placed at 900 cm^{-1} by analogy with the F-O bond in $FONO_2$, since the mass of the fluorine atom is nearly the same as that of the ammonia ion.

The value of the frequency variation for AN was $(v/\omega_i)\, d\omega_i/dv$ = 0.028721326.

TABLE 1. VIBRATIONAL MODES OF AMMONIUM NITRATE

mode	wavenumber (cm^{-1})	degeneracy
O-H bending	1300	1
O-H stretching	3700	1
NH_3 umbrella	1400	3
NH_3 stretch (as)	3145	2
NH_3 scissor	1680	2
NH_3 stretch (s)	3040	1
O-NH_3 torsion	150	1
O-NO_2 torsion	456	1
O-NO_2 i.p. bend	710	1
O-NH_3 bending	300	2
N-O bending	450	1
N-O bending	630	1
NO_2 scissor	800	1
O-NH_3 stretching	900	1
NO_2 stretch (s)	1300	1
NO_2 stretch (as)	1760	1

Rotations and translations of the whole molecule are not included in the table.

A heat capacity of kT per mode was associated with translational and rotational modes of the molecule to allow for kinetic and potential contributions.

The vibrations were combined with the cold curve as discussed above to obtain a thermodynamically complete EOS.

Using the vibrational frequencies, the specific heat capacity at constant volume c_v for the STP state was predicted to be 1220 J/kg.K. The observed heat capacity at constant pressure c_p is 1740 J/kg.K [20]. In general, c_v is greater than c_p, by an amount kT per molecule for a perfect gas [21]. The difference here is somewhat greater than might be expected for a solid. We are investigating the discrepancy.

The Hugoniot obtained from the quasiharmonic EOS reproduced the Grüneisen fit reasonably well.

POROUS AN

As discussed above, initial porosity can be treated explicitly using the mixture model. A significant advantage for continuum simulations is that no further adjustments are needed to predict the effect of changes in porosity, beyond choosing the initial volume fraction for the pore gas. The evolution of porosity under different loading histories (e.g. multiple shocks) is also handled seamlessly. This approach is significantly more convenient than applying empirical adjustments to the Hugoniot [22, 23, 24], and it appears to be at least as accurate.

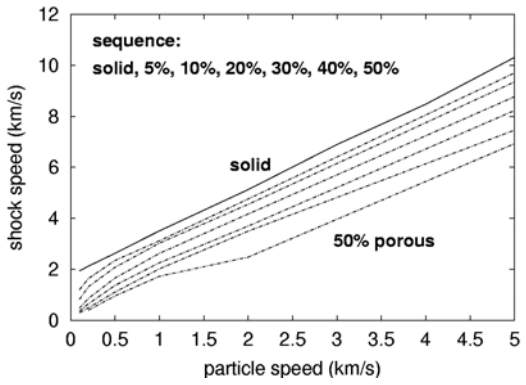

FIGURE 1: AN: POROUS HUGONIOTS PREDICTED USING QUASIHARMONIC EOS AND IDEAL EQUILIBRATION (INFINITE-SIMAL PARTICLE SIZE).

Predictions were made of the porous Hugoniot for AN by performing hydrocode simulations of shock propagation in the porous material with different piston velocities applied at one end, and using air (represented by a perfect gas EOS) as the pore gas. Shock speeds were determined using the artificial viscosity q from the position of the maximum in q/ρ as a function of time. At higher porosities and lower pressures the shock broadened into a gradual compaction which took some time to become steady. There was thus some uncertainty in the velocity (probably responsible for the kink at 50% porosity) though as consistent a method as possible was used. (Fig. 1.)

The heterogeneous mixture method described here accurately modelled subtle details of the porosity-dependent initiation behavior of HMX-based military explosives, where the porosity was ~1% or less [2,3]. In AN, numerical problems were encountered in a previous two-component mixture model [27] for porosities above about 15%, apparently caused by regions of state space in which the sound speed became imaginary. The problems could be ameliorated but not removed by adjusting the equations of state of the product gases. The improved model described here was found to operate with porosities up to at least 50%.

Ideally, we would like to calibrate models of mechanical response and reaction to data from 1-D shock wave experiments. Suitable data exist for the Hugoniot of 45% porous AN. [22] The particle velocity u_p, and shock velocity u_s were measured directly using electromagnetic velocity gauges [25]. In one of the experiments, reaction was observed, providing an experimental run distance for shock initiation.

The calculated Hugoniot was not sensitive to the equilibration rates or mesh size, and was unchanged on using a SESAME EOS for the pore gas instead of the perfect gas EOS. Excellent agreement could be obtained by using the Steinberg EOS more directly, with a cold curve and constant heat capacity to provide an estimate of the temperature. The difference between the quasiharmonic EOS and the data is thus likely to reflect the deviation between the quasiharmonic EOS and the Grüneisen form. We prefer the quasiharmonic EOS for simulations of reactive flow because the temperatures are much more likely to be accurate. (Fig. 2.)

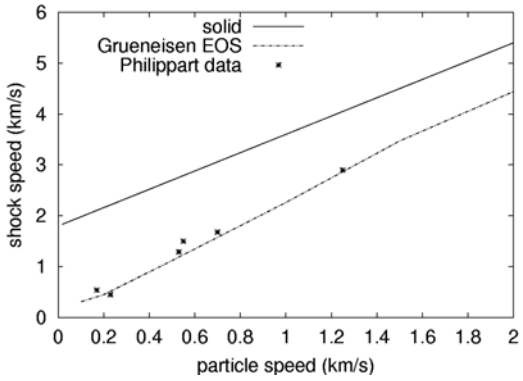

FIGURE 2: AN HUGONIOT, 45% POROSITY.

EQUATION OF STATE FOR FUEL OIL

The fuel oil was taken to be an olefin, composition C_nH_{2n+2}, with a molecular weight of $14n + 2$. The chain length n is almost immaterial, but it provides a mechanism for counting atoms. We used $n = 10$ for convenience.

The equation of state for fuel oil (FO) was obtained by the same method used for AN. No compression data were found for fuel oil, so we assumed that the properties would be similar to those of paraffin, for which Hugoniot data have been published [14]. Steinberg's form of Grüneisen EOS was fitted to the data as discussed above. In contrast with the published fits for AN, non-linear terms were needed to represent the paraffin data.

The Hugoniot was fitted with a cubic Grüneisen form, with parameters c_0=1.8034 km/s s_1 =3.56525, s_2 =-5.2109, and s_3 =2.82867. Grüneisen's Γ was taken to be constant, 2.04846.

The density at STP, ρ_0 = 0.9185g/cm^3. The density at $T = 0$, $p = 0$ (ρ^0_0) was estimated to be 0.964425g/cm^3, a 5% decrease from the STP value.

As with AN, molecular vibrations were used to modify the cold curve, to produce a Hugoniot at finite temperatures.

Fuel oil is modelled by saturated single chain

olefins C_nH_{2n+2}, where n may vary. For n carbons, we expect $9n$ vibrational modes. In order to determine a generic spectrum, the infrared spectra of various structural isomers of C_4H_{10} and C_6H_{14} were compared. [10] In molecules such as hexane, the exact configuration (cis- or trans- at each C-C bond) determines the frequencies, to within about 30 to 50 cm^{-1}. As a variety of configurations can be anticipated, the frequencies were grouped into bands of between 40 cm^{-1} and 100 cm^{-1} in width, on the assumption that the large number of configurations present will provide an average approximately equal to the center of the band, the frequency used. The larger the molecule, the more normal modes occur, and accordingly, the number of frequencies falling within each band is expressed in terms of the chain length, n. Where the number of frequencies could not in practise be determined from a knowledge of the molecular vibration principally responsible for the frequencies, e.g. hydrogen stretching modes or carbon skeletal bends, the number of frequencies was estimated by comparison of a number of spectra of different molecules. [10]

TABLE 2: VIBRATIONAL MODES FOR C_nH_{2n+2} MOLECULE, "FUEL OIL"

mode	wavenumber (cm-1)	width (± cm-1)	degeneracy
Torsion	200	100	*n-1*
Skeletal bends	400	100	*n-1*
CH_2 rock	760	40	*n/2*
CH_3 rock	900	50	*n-2*
C-C stretches	1050	40	*n-2*
CH_3 deform	1140	10	*2*
CH_2 twist	1250	30	*n/2*
CH_2 wag	1350	10	*n*
CH_2 scissor	1450	30	*n+2*
CH stretches	2900	50	*2n+2*

Rotations and translations of the whole molecule are not included in the table.

As for the AN, the change in frequency as a function of pressure was described, in the absence of high pressure vibrational spectra, by a single value for all modes. The value of $(v/\omega_i)\, d\omega_i/dv$ necessary to reproduce the STP state was 0.035476.

The Hugoniot produced from the quasiharmonic equation of state was a reasonable fit to the Marsh data up to about 20 GPa. At higher pressures, the calculated Hugoniot fell below the data. As with AN, there are several possible explanations: the cold curve calculated using the Grüneisen model may be too soft; the vibrational frequencies may increase too slowly with compression in this region; or the quasiharmonic assumption may break down as compression or temperature increase because of mixing of the modes, caused by the large number of modes and the small energy differences between them. (Fig. 3.)

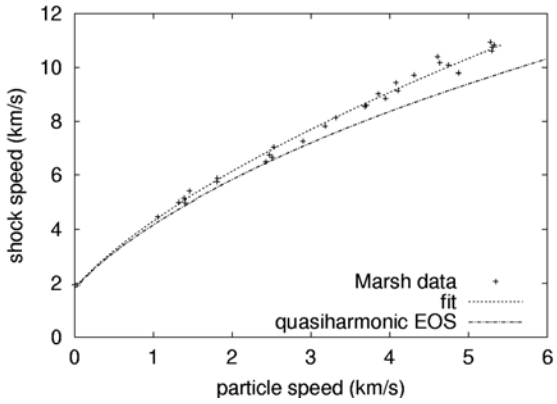

FIGURE 3: HUGONIOTS FOR PARAFFIN

EQUATIONS OF STATE FOR REACTION PRODUCTS

The products equation of state was generated using the chemical equilibrium code CHEETAH, [26] with EXP-6 potentials. SESAME-type [8] EOS were calculated for compositions between pure AN and pure FO, concentrating on the range from 90 to 100% AN by mass. The form of the EOS was thus $\{p,T\}(\rho, e, \lambda)$, where λ is the mean fraction of fuel oil.

REACTION RATES

A generalized Arrhenius form was used for the local chemical reaction rates:

$$\lambda^{\bullet} = R_0 \exp(-T^*/T) \qquad (12)$$

where T^* is the activation energy for reaction, and R_0 is the attempt frequency for effective collisions. T^* and R_0 may be functions of P and T, though in the present work constants were used. Further investigation of the coefficients in the rate might permit the model to reproduce steric hindrance and other physical phenomena that may limit the activation of a particular chemical reaction [28].

We used the temperature determined on the Hugoniot defined by the equilibrated vibrations to govern the reactions of the molecule, assuming absence of mode-specific excitation producing reaction. [29,30]

As discussed above, we included a surface burn contribution to the reaction rate. The

Arrhenius rate was used to predict when significant surface burning would occur, and a flame propagation model was used in this situation. The flame speed would ideally be calibrated by mesoscale simulations of reaction with heat conduction; here we chose a constant value of the flame speed and investigated the sensitivity of run distance to different choices. The surface contribution required an estimate to be made of the relation between the common surface area α_{ij} between each pair of components and the volume fraction of each. We estimated this relation using a functional of the volume fraction of each:

$$\alpha_{ij} \propto f_i^{2/3} f_j^{2/3} . \qquad (13)$$

The constant of proportionality was obtained by using the grain size to estimate the number density of grains, and calculating their approximate surface area between two components of $f_i = f_j = 1/2$.

The energy release on reaction was determined from thermodynamic tables of the enthalpy of formation [31, 32].

CALIBRATION FOR AN

Limited run distance data exist for porous AN. [22] The run distance for AN of 45% porosity was observed to be ~4 to 5 mm when initiated at a particle speed of 1.18 km/s. The Arrhenius rate for AN alone was calibrated against this data.

The pressure applied to give the observed particle speed was calculated using the unreactive porous model to be 3.0 G Pa. The modal grain size was 250 μm, [22] suggesting a time scale for pressure equilibration ~0.1 μs. The time scale for thermal equilibration was taken to be an order of magnitude larger. The modal grain size was also used to estimate the magnitude of the surface area contribution to the reaction rate.

As a starting point, the frequency factor R_0 was taken to be 10^{14} /s, which is a typical frequency of atomic vibration. The activation energy T^* was then adjusted by simulating shock initiation until the run distance was similar to the observed value.

We found that a run distance of the correct order was given with $T^* \sim 12500$ K. Simulations were used to predict the run distance as a function of drive pressure and porosity (Fig. 4). The equilibration rates made a significant difference if changed by an order of magnitude. The sensitivity of drive pressure and porosity (Fig. 4). The equilibration rates made a significant difference if changed by an order of magnitude. The sensitivity to mesh size was found to be very close to linear. Run distances converged to ~0.5 mm or better with a mesh size of 0.1 mm.

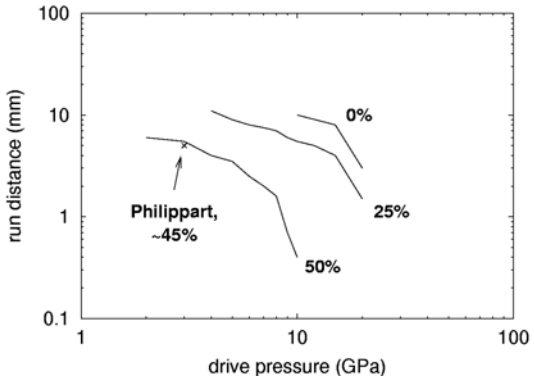

FIGURE 4: POP PLOTS FOR AN OF DIFFERENT POROSITY. NO SURFACE REACTIONS, τ_p = 0.1 μs, τ_t = 1.0 μs, MESH SIZE = 0.1 mm.

CALIBRATION FOR ANFO

For the purposes of demonstration, calibration and comparison with ANFO was done using the formulation RX-HD, for which Lee-Tarver initiation parameters have been calculated [33]. Lee-Tarver simulations of shock initiation were used as run distance data, though this approach should be treated with caution since the Lee-Tarver parameters applied to overdriven detonation.

By mass, RX-HD contains 78.65% AN, 9.45% water, 5.52% calcium nitrate, 6.38% fuel oil, and 0.08% plastic microballoons. This composition is sufficiently complicated that mixing or EOS problems are likely to obscure effects from the reactive flow model, so a simplified composition was considered for the calibration. We took proportions by mass of 78.65 AN to 15.83 fuel oil, giving mass fractions of 83% and 17% respectively. In our reactive flow model the components are specified by volume; these mass fractions correspond to volume fractions of 72% and 28% respectively. The microballoons control the porosity, but the mass of the plastic wall makes it difficult to infer a porosity directly. We assumed that the difference between the mass density of the simplified mixture and that of RX-HD was accounted for by the porosity a reasonable assumption which gave a porosity ~12%. The volume fractions of the condensed components were reduced proportionately, and the pore volume modelled as gas. As discussed above, the pore gas was taken to be AN decomposition products at STP, though simulations were also performed using EOS for air to investigate any sensitivity.

The initiation behaviour of the model was not sensitive to the EOS used for this initial pore gas.

Ideally, we would hope for the simulations to agree with the 'data' — which was in this case another simulation based on an empirical model extrapolating outwith its probable range of validity.

PREDICTED SHOCK SENSITIVITY FOR RX-HD

The model for RX-HD was used to predict the variation of run distance with driving pressure. As discussed above, these predictions were compared with Lee-Tarver simulations intended to represent empirical data. The simulations also used a mesh size of 0.1 mm. Run distances were obtained by inspection of graphs of the position-time history of the leading shock. These estimates were accurate to about 0.5 mm.

The decomposition of fuel oil was modelled using a frequency factor of 10^{14} /s and T* ~ 15000K. The run distance was not very sensitive to the rate for decomposition of the fuel oil. T* was chosen to be 15000K, which permitted decomposition to occur in a reasonable time. This model predicted a run distance which was systematically longer than the Lee-Tarver results; since a simplified representation of RX-HO was used this is an encouraging level of consistency. (Fig. 5)

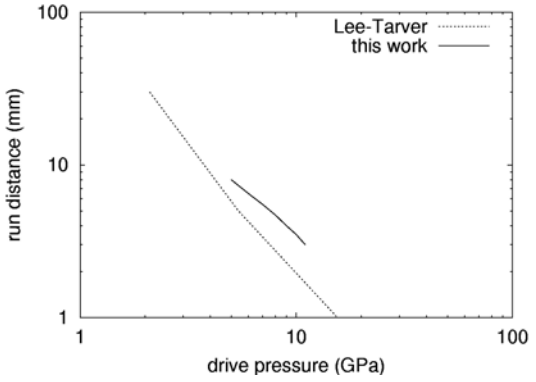

FIGURE 5: POP PLOTS FOR ANFO COMPOSITION RX-HD.

CONCLUSIONS

A physically-based reactive flow model for ANFO explosives has been developed, based on a previous heterogeneous model developed for HMX-based explosives. [2,3] The model uses thermodynamically complete equations of state and Arrhenius reaction rates with a surface burn term representing the effect of the hotspots.

Condensed phase equations of state were predicted from shock wave data and estimates of the vibrational modes in each type of molecule. The resulting quasiharmonic equations of state were fairly consistent with the shock wave data, but could usefully be improved by adjusting the cold curve and using a more detailed treatment of the variation of vibrational frequencies with compression.

Porosity was modelled explicitly by including a volume fraction of gas in the virgin material. AN Hugoniots were predicted for porosities up to 50%, and compared with experimental data at 45%. The quasiharmonic EOS provided a reasonable fit to the data; an empirical EOS fitted to the shock wave data for solid AN gave excellent agreement with the porous data, again suggesting that the quasiharmonic EOS should be adjusted slightly to improve its match to the solid Hugoniot. However, the porosity model itself appears to be perfectly adequate even at these rather large distensions, and it is recommended for continuum mechanics simulations.

The model can predict the effect of changes in composition, porosity, and particle size on the run to detonation as a function of loading conditions. Within the limitations of the sparse EOS and reaction data used for calibration, predictions made using the model are comparable with empirical data. The advantage of this model is that it allows initiation properties to be predicted from the properties of the components of a heterogeneous explosive, rather than requiring the behaviour to be measured for each new composition and morphology.

We plan eventually to perform simulations for other fuels, and to include additional short-lived chemical species, allowing us to predict the effect of chemical desensitisers.

Detailed kinetic observations may be used to guide the selection of Arrhenius constants, particularly R_0, allowing steric hindrance and other detailed mechanisms to be addressed. Competitive multiple pathways may be included directly.

REFERENCES

1. D. L. Kennedy, *Multi-valued normal shock velocity versus curvature relationships for highly non-ideal explosives,* Proc. 11th International Detonation Symposium, held Snowmass, Colorado, USA, 30 Aug to 4 Sep 1998, ONR 33300-5 (2000).

2. R. N. Mulford and D. C. Swift, Proc. International Workshop on Non-Ideal Explosives, Socorro, NM, USA, Mar 1999, EMRTC (2000).

3. R.N. Mulford and D.C. Swift,, Proc APS

Topical Conference on Shock Compression of Condensed Matter, Snowbird, Utah, USA, Jun 1999, AlP (2000).

4. N. Whitworth and J. Maw, Proc APS Topical Conference on Shock Compression of Condensed Matter, Snowbird, Utah, USA, Jun 1999, A lP (2000).

5. G. Wanstall (QINETIC Fort Halstead), private communication (2001).

6. M. Chaudhri and J. E. Field, Proc Roy Soc A340, 113 (1974).

7. R.N. Mulford and D.C. Swift, Proc APS Topical Conference on Shock Compression of Condensed Matter, Atlanta, GA, 25 to 29 Jun 2001.

8. K.S. Holian, *T-4 Handbook of Material Properties Data Bases, Vol.* 1 c: *Equations of State,* Los Alamos National Laboratory report LA-10160-MS (1984).

9. K. Nakamoto, "Infrared and Raman Spectra of Inorganic and Coordination Compounds, 4th Edition." John Wiley and Sons, Inc. 1986.

10. T. Shimanouchi, "Tables of Molecular Vibrational Frequencies, NSRDS NBS 39, Nat. Stand. Ref. Data Ser., Nat. Bur. Standards (U.S.), 39, 1972. And "ibid., Part 9," Journal of Physical and Chemical Reference Data, 7(4), p. 1323-1443 (1977).

11. R.N. Mulford and D.C. Swift, *Reactive Flow Models for Nitromethane,* in Proc. International Workshop on New Models and Hydrocodes for Shock Wave Processes in Condensed Matter, Edinburgh, Scotland, !9-24 May, 2002.

12. D. J. Steinberg, , Lawrence Livermore National Laboratory report UCRL-MA-106439 change 1 (1996).

13. I.C. Skidmore, Applied Materials Research pp 131 –147 (July 1965).

14. S.P. Marsh (Ed), "LASL Shock Hugoniot Data", University of California (1980).

15. D.C. Swift, Los Alamos National Laboratory report LA-UR-01-3005 (2001).

16. J. M. Winey, G. E. Duvall, M. D. Knudson and Y. M. Gupta, , J. Chem. Phys. vol. 113 no.17 pp 7492- 7501 (2000).

17. F. Sandstrom, *Equation of state of ammonium nitrate and ammonium perchlorate,* MSc Thesis, EMRTC, New Mexico Tech., USA, Dec. 1994.

18. Courchinoux and P. Lalle, High Pressure Science and Technology, 1993, published by the American Institute of Physics, Woodbury, NY, pp. 1397-1398.

19. J. R. Ferraro, "Vibrational Spectroscopy at High External Pressures," Academic Press, Inc., Orlando, Florida, 1984.

20. G.C. Pimentel and R.S. Spratley, "Understanding Chemistry," Holden-Day, San Fransisco (1971).

21. J. R. Waldram, "Introduction to thermo-dynamics," Cambridge (1984).

22. D. A. Philippart and S. G. Hookings, in Proc. of the International Workshop on Non-ldeal Explosives, held Socorro, NM, USA, Mar 1999, EMRTC (2000).

23. N. Asfanasenkov, V. M. Bogomlov and I. M .Voskoboinikov, Zh. Pikl. Mekh. Fiz. 10, p. 660, 1970.

24. Thouvenin,, Proc. 4th Symposium. (Int.) on Detonation 1965, pp. 258-265, White Oak, Springfield, Maryland, USA; see also Meyers, *Dynamic behavior of materials,* John Wiley and Sons, 1994.

25. D. Philippart, in *8th Symposium (International) on Detonation, Albuquerque, New Mexico, USA, July* 1985 pp. 447-459.

26. L.E. Fried, W.M. Howard, P.C. Souers, and P.A. Vitello (Lawrence Livermore National Laboratory), documentation for CHEETAH version 3.0 (2001.)

27. R.N. Mulford and D.C. Swift, Proc. Interna-tional Workshop on Non-Ideal Explosives, Socorro, NM, USA, May 2001, EMRTC (2001).

28. K. Yeager, "Urea-nitric acid system" ibid,

29. D..D. Dlott and M.D. Fayer, J. Chem. Phys., 92, 3798, (1990).

30. C. B. Moore and I. W. M. Smith,, Faraday Discussions, Chem Soc **67'** 196 (1979).

30. G. C. Pimentel and R. S. Spratley, "Under-standing Chemistry," Holden-Day, San Francisco (1971).

32. Lange's Handbook of Chemistry, 44th Edition.

33. P.C. Souers and L.C. Haselman Jr., Lawrence Livermore National Laboratory report UCRL-m-116113 (1994).